Huang, Haibing; Modanese, Chiara; Sun, Shenghua; von Gastrow, Guillaume; Wang, Jianbo; Pasanen, Toni P.; Li, Shuo; Wang, Lichun; Bao, Yameng; Zhu, Zhen; Sneck, Sami; Savin, Hele

Effective passivation of p^+ and n^+ emitters using $SiO_2/Al_2O_3/SiN_x$ stacks: Surface passivation mechanisms and application to industrial p-PERT bifacial Si solar cells

Published in:
Solar Energy Materials and Solar Cells

DOI:
10.1016/j.solmat.2018.07.007

Published: 01/11/2018

Document Version
Peer-reviewed accepted author manuscript, also known as Final accepted manuscript or Post-print

Effective Passivation of p^+ and n^+ Emitters Using $SiO_2/Al_2O_3/SiN_x$ Stacks: Surface Passivation Mechanisms and Application to Industrial p-PERT bifacial Si Solar Cells

Haibing Huang[1,2*], Chiara Modanese[2], Shenghua Sun[1], Guillaume von Gastrow[2], Jianbo Wang[1], Toni P. Pasanen[2], Shuo Li[2,3], Lichun Wang[1], Yameng Bao[2], Zhen Zhu[2,3], Sami Sneck[3], Hele Savin[2]

1. China Sunergy, No.123. Focheng West Road, Jiangning Zone, Nanjing, Jiangsu, 211100, China

2. Aalto University, Department of Electronics and Nanoengineering, Tietotie 3, 02150 Espoo, Finland

3. Beneq Oy, P.O. Box 262, 01511 Vantaa, Finland

*Corresponding author: Tel.: +86-15850677052; E-mail address: huang.haibing@aalto.fi

Abstract- In this paper, we present an effective emitter passivation scheme using $SiO_2/Al_2O_3/SiN_x$ stacks. Our study shows that $SiO_2/Al_2O_3/SiN_x$ stacks can well passivate both p^+ and n^+ emitters due to an excellent chemical passivation combined with a weak field-effect passivation. Good quality boron and phosphorus emitters were achieved over a broad emitter-doping range, as demonstrated by post-fired emitter saturation current of 20 and 30 $fA \cdot cm^{-2}$, respectively. Based on the results obtained with $SiO_2/Al_2O_3/SiN_x$ emitter passivation, we present an industrial roadmap for a p-PERT bifacial cell structure. Using this roadmap, we demonstrate industrial p-PERT bifacial cells with front side efficiency of 20.5%, rear side efficiency of 19.8% (bifaciality factor *BF*=0.98) for rear textured cells and 17.5% (*BF*=0.85) for rear planar cells. In particular, the cells with bifacial $SiO_2/Al_2O_3/SiN_x$ passivation on both p^+ and n^+ emitters also demonstrate promising performance and a simplified cell process. The results show that $SiO_2/Al_2O_3/SiN_x$ emitter passivation scheme is a promising candidate for photovoltaic industry.

Index Terms— Al_2O_3, boron emitter, PERT, phosphorus emitter, SiO_2, surface passivation

1. Introduction

As photovoltaic (PV) energy is to become one of the main renewable energy sources in the next decades, the industry needs to pay attention to mass production of cost-efficient solar cells. Emitter (n^+ and p^+) passivation is an important step towards this goal. Dielectric films, e.g. SiN_x [1–3], Al_2O_3 [4–8] and SiO_2 [1,9–15], can well combine both field-effect and chemical passivation, and as a result they have been successfully applied into surface passivation of crystalline Si (c-Si) solar cells in the lab and industry. For surface passivation from the solar cell operation point of view, the most important benchmark is to achieve a good "final" passivation, i.e. after co-firing for screen-printed Si solar cells, rather than a good initial or intermediate passivation. It is well known that single layer dielectric passivation such as Al_2O_3 or SiO_2 tends to suffer from firing stability issues [7,16–20]. This means that a high intermediate passivation level during cell processes can be obtained, but it cannot be maintained when cell fabrication is completed. Previous studies indicate that the poor firing stability of thin Al_2O_3 (< 20 nm) is attributed mainly to an increase in interface defect density (D_{it}) while fixed charge density (Q_f) of Al_2O_3 is found to be less affected [7,16]. Further, the increased D_{it} is due to dissociation of interfacial Si–hydrogen bonds at elevated temperatures [21]. A thicker Al_2O_3 (e.g. >30 nm) can improve firing stability to some extent, however such thick films suffer from blistering [22,23] and are not cost-efficient. Dielectric stacks, e.g. SiO_2/SiN_x, Al_2O_3/SiN_x, can improve the final passivation, which has been attributed mainly to hydrogen (H) passivation provided by the stacks [7,17,21,24–26].

Another surface passivation candidate with a good firing stability are SiO_2/Al_2O_3 stacks, which have been recently studied by some groups. According to Ref.s [27–31], the space-charge field can be regulated via tuning the effective charge density (Q_{eff}) of the whole stacks by changing the SiO_2 interlayer thickness (d_{SiO2}). Furthermore, SiO_2/Al_2O_3 stacks can provide H passivation and thus a good chemical passivation of the Si interface [32–35]. The interfacial SiO_2 is crucial for the excellent chemical

passivation [4,7,36,37] and it can be either grown in-situ during atomic layer deposition (ALD) and post-anneal or grown ex-situ using a separate thermal oxidation, ALD, plasma enhanced chemical vapor deposition (PECVD) and chemical oxidation processes [4,7,28,30,36,38]. Thus, due to an excellent chemical passivation combined with a weak field-effect passivation, SiO_2/Al_2O_3 can well passivate both n-Si [29,32,39–41] and p-Si [29,30,42]. Despite the extensive material-level studies on SiO_2/Al_2O_3 stacks, their application in screen-printed industrial Si solar cells is limited. This requires systematic studies on changes in passivation mechanisms during cell fabrication processes and their impact on cell performance. Moreover, since SiO_2/Al_2O_3 can well passivate both n^+-Si and p^+-Si, it should bring a clear cost benefit in various cell structures such as IBC (Interdigitated Back Contact) [14], PERT (Passivated Emitter and Rear Totally-diffused) [11,12] and bifacial cells.

In this paper, we study the applicability of $SiO_2/Al_2O_3/SiN_x$ stacks to screen-printed industrial Si solar cells. We start by studying the emitter passivation mechanisms of different stacks, namely Al_2O_3, Al_2O_3/SiN_x, SiO_2/Al_2O_3, $SiO_2/Al_2O_3/SiN_x$ and SiO_2/SiN_x, with special focus on the changes caused by the thermal treatments typically present in industrial solar cell fabrication, as well as in pursuit of the best final (after firing) emitter passivation quality. Then we apply the optimized $SiO_2/Al_2O_3/SiN_x$ stacks to p-PERT bifacial cells. While p-PERT bifacial cells may seem somewhat expensive cell architecture due to relatively immature boron doping technology, especially when compared to bifacial $PERC^+$ cells [43] that are based on more mature industrial PERC (Passivated Emitter and Rear Cell [13]) concept, p-PERT bifacial structure has the following benefits: 1) under this premise of the same front-side cell efficiency, boron-doped back-surface field (BSF) provides higher rear-side cell efficiency (thus higher bifaciality factor [44]) than Al doping; 2) the compatibility of structure and process with n-PERT and 3) the studied $SiO_2/Al_2O_3/SiN_x$ stacks can passivate both boron (B) and phosphorous (P) emitters present in the structure.

2. Experimental

In this study, both minority carrier lifetime (hereinafter shortened as lifetime) and solar cell experiments were carried out. For the B-emitter lifetime experiments, we used pseudo-square 6-inch Czochralski (Cz) n-Si wafers from the same ingot, with bulk resistivity $\rho_{bulk}\approx 2\ \Omega\cdot cm$ and a starting thickness of 190 μm. For the P-emitter lifetime experiments and cell experiments, we used standard pseudo-square 6-inch Cz p-Si wafers with ρ_{bulk} = 2-3 Ω·cm and a starting thickness of 190 μm, taken from the same ingot. The lifetime and cell samples are 5 and ~50 for each group, respectively.

The sequence of the lifetime experiments is shown in Fig. 1. Symmetrical p^+np^+ (n^+pn^+) samples were prepared to investigate the passivation quality of p^+ (n^+) emitters. After saw damage removal (SDR) using NAOH solution and a pre-cleaning using HCl-HF solution, B or P implantation was performed using Intevac's ENERGi industrial implanters and it was followed by an in-situ oxidation anneal in a tube furnace. The B implantation used B_2H_6 (15% B_2H_6 + 85% H_2) as the ion source with the implant energy E=10 keV, dose D=1.3-3.8·10^{15} cm^{-2} and anneal temperature T=1050°C. The P implantation used PH_3 (100% pure) as the ion source with the E=7 keV, D=2.2-3.5·10^{15} cm^{-2} and anneal T=840°C. After etching the thermally grown SiO_2 using dilute HF solution, sheet resistance $R_{\square}$ of B emitter ($R_{\square B}$) and P emitter ($R_{\square P}$) was measured by four-point probe on n-Si and p-Si monitor wafers, respectively. Junction profiles and parameters (surface doping concentration N_{surf}, junction depth X_j) were measured using secondary ion mass spectroscopy. The N_{surf} are electrically activated by confirming with Ssuprem3.1 simulations via comparing the total and active dopants profiles. Al_2O_3 or Al_2O_3/SiN_x stacks were then deposited on the wafers for further passivation. A dilute HCl-HF pre-Al_2O_3 clean was performed for the $Al_2O_3/(SiN_x)$ stacks, while no pre-clean was performed for the $SiO_2/Al_2O_3/(SiN_x)$ stacks. Al_2O_3 was

deposited using Beneq's P800 industrial batch thermal ALD with $Al(CH_3)_3$ trimethylaluminium (TMA) and ozone (O_3) precursors, T=200ºC and 10 nm (90 cycles) film thickness. Post-Al_2O_3 anneal was performed in a tube furnace in N_2 atmosphere at 425°C for 25 min. SiN_x was deposited using Roth-Rau's parallel-plate type PECVD ($SINA^L$) at 400°C. Rapid thermal process (RTP) firing was performed using Despatch's (Ultraflex) firing furnace, with the real peak T≈750°C, belt speed≈6250 cm/min and in compressed air.

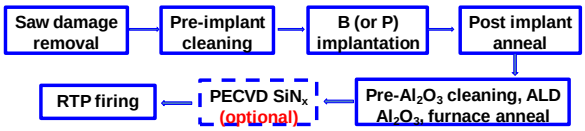

Fig. 1. The sequence of the lifetime experiments in this study.

Effective lifetime and emitter saturation current (J_{0e}) were determined by photo conductance decay using a Sinton WCT120 tester [45]. The basic settings are: 1) generalized mode; 2) $5 \cdot 10^{15}$ cm^{-3} specified minority carrier density (MCD) for effective lifetime measurement; 3) J_{0e} extracted using Kane and Swanson's method [46] by selecting a suitable MCD within the emitter recombination-dominant region (typical range of ±30% around 10× the base doping concentration) to well match the fitted J_{0e} curves; 4) optical constant selected depending on reflectance and transmittance of Si surface and dielectrics (0.7 for (100)-oriented Si surface, 0.7-0.95 for $(SiO_2)/Al_2O_3/(SiN_x)$) [45]. By combining the Sinton tester with iodine passivation [47], the measured bulk lifetime of the used Cz n-Si and p-Si is ~750 and ~250 µs, respectively. Film thickness (d_{film}) and refractive index were measured with a Suntech ellipsometer at a wavelength of 633 nm. Q_{eff} of dielectrics was measured by Semilab SDI PV2000 using the contactless COCOS (corona oxide characterization of semiconductors) method [48]. In this study, Q_{eff} is defined as the sum of the total negative and positive charge density in the dielectrics that causes the space-charge field in the Si. Because Q_{eff} cannot be directly measured on the emitter surface using the COCOS method, we instead measured Q_{eff} on p-Si and n-Si wafer substrates to evaluate p^+ and n^+ emitter, respectively.

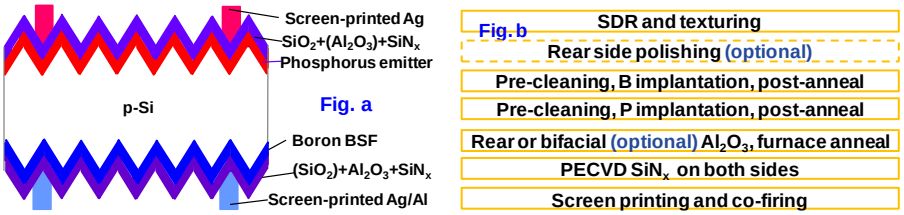

Fig. 2. The p-PERT bifacial cell structure (rear textured surface sketched) and process.

The p-PERT bifacial cell structure and process are shown in Fig. 2. The cell rear surface was designed as textured or planar based on different application requirements. After SDR and random-pyramids texturing, the cell rear was optionally (i.e. for some groups of the wafers) single side polished using HNO_3-HF-H_2SO_4 solution in a RENA's (RENA InOxSide HT) wet bench. Front n^+ emitter ($R_{\square P}$=88 Ω/□) and rear p^+ BSF ($R_{\square B}$=69 Ω/□) were formed via P and B implantation and post implantation anneal. During the post P implantation anneal, a thin SiO_2 was grown in-situ to passivate the implanted junctions on both sides. PECVD SiN_x or ALD Al_2O_3/PECVD SiN_x were deposited on both sides of the cells for antireflection (ARC) and surface passivation. Al_2O_3 process was followed by a furnace anneal in N_2 atmosphere at 425°C for 25 min. Screen printing and co-firing were used for metallization (5 busbars each side). In addition, the pre-Al_2O_3 treatments were: 1) the thin SiO_2 in the $SiO_2/Al_2O_3/SiN_x$ stacks was

grown in-situ during the post P implantation anneal and no pre-cleaning was performed on cells with $SiO_2/Al_2O_3/SiN_x$; 2) for cells with p^+ emitter/Al_2O_3/SiN_x, a ~68 nm SiN_x was deposited on the cell front after the post P implantation anneal, to protect the front SiO_2 in the subsequent pre-Al_2O_3-cleaning. Before Al_2O_3 process, the rear thin SiO_2 was removed by a dip in 0.5% HF+HCl solution for ~15-30 s, during which the front 68 nm SiN_x was etched <1 nm. The as-fabricated cell performance of front side (under front illumination only) and rear side (under rear illumination only) were independently measured with a Berger I-V tester under standard global AM1.5 spectrum, 1000 $W \cdot m^{-2}$, at 25 ºC.

3. Result and Discussion

3.1 Lifetime results: effective $SiO_2/Al_2O_3/SiN_x$ passivation on B and P emitter

In order to implement the lifetime results to the solar cells, the d_{film} of each layer of the stacks and thermal treatments were designed considering the practical limitations related to cell structure and process. Hence, the lifetime results can reflect to some extent the cell performance.

First, we study the passivation of B emitter. The J_{0e} of B emitter (hereinafter denoted as $J_{0,p+}$) with different stacks as a function of the undergone thermal processes, is shown in Fig. 3. Right after the Al_2O_3 process, there is scarcely any passivation effect on the B emitter without SiO_2, while there is weak passivation provided by the 7 nm SiO_2. Only considering the $J_{0,p+}$ after the post-Al_2O_3 furnace anneal (hereinafter denoted as PAFA), $Al_2O_3/(SiN_x)$ is significantly better than $SiO_2/Al_2O_3/(SiN_x)$. The increased $J_{0,p+}$ of each group after PECVD SiN_x is due to the plasma bombardment induced damage on Al_2O_3. The subsequent firing can both cure this damage and promote H passivation from the stacks, leading to a significantly recovered passivation level. The post-fired $J_{0,p+}$ with SiO_2 is clearly better than without SiO_2. Furthermore, a SiN_x capping layer can further decrease $J_{0,p+}$. It was confirmed in our study [23] that, for the stacks used here, ≤10 nm ALD Al_2O_3 (TMA and O_3 based) scarcely suffers from blistering after undergoing the thermal processes in the lifetime and cell experiments. Thus, the better post-fired $J_{0,p+}$ of $SiO_2/Al_2O_3/(SiN_x)$ cannot be attributed to a reduced blistering problem. Overall, the results indicate that the thin SiO_2 between p^+-Si and Al_2O_3 as well as the SiN_x capping layer can improve the firing stability of Al_2O_3, thus decreasing $J_{0,p+}$.

The corresponding J_{0e} results on P emitter ($J_{0,n+}$) are shown in Fig. 4. The J_{0n+} after PECVD SiN_x is not shown since it has a similar trend as $J_{0,p+}$ (Fig. 3). In all cases, bare $Al_2O_3/(SiN_x)$ provided poor passivation, while $SiO_2/Al_2O_3/(SiN_x)$ achieved good $J_{0,n+}$, especially after firing (even slightly better than SiO_2/SiN_x). Similarly to B emitters, a SiN_x capping layer further decreases $J_{0,n+}$. Overall, the results indicate that the thin SiO_2 between n^+-Si and Al_2O_3 is critical to decrease $J_{0,n+}$, and that the SiN_x capping layer can improve the firing stability of Al_2O_3.

Fig. 5 shows the $J_{0,p+}$ ($J_{0,n+}$) and active N_{surf} as a function of $R_{\square}$ and different stacks. Over a broad $R_{\square B}$ range, the $Al_2O_3/(SiN_x)$ stacks could achieve a good J_{0p+} right after PAFA, but they did not maintain it after firing, thus implying a cell performance loss. In comparison, the $SiO_2/Al_2O_3/SiN_x$ stacks achieved a good final post-fired $J_{0,p+}$ or $J_{0,n+}$ over a broad $R_{\square}$-range, as demonstrated by post-fired $J_{0,p+}$ = 20-50 $fA \cdot cm^{-2}$ with $R_{\square B}$-range of 115-60 Ω/□ and post-fired $J_{0,n+}$ = 30-50 $fA \cdot cm^{-2}$ with $R_{\square P}$-range of 100-70 Ω/□. It is worth noting that, such results were also found in BBr_3- or $POCl_3$-diffused emitters in our unpublished study. The above results are also consistent with Ref.s of [29,30,32,39–42], which have mainly focused on the lab-scale research and are based on different research perspectives, showing effective surface passivation of p-Si and n-Si using $SiO_2/Al_2O_3/(SiN_x)$ synthesized by various methods.

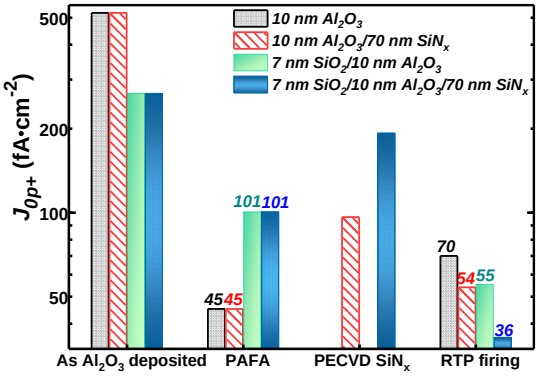

Fig. 3.

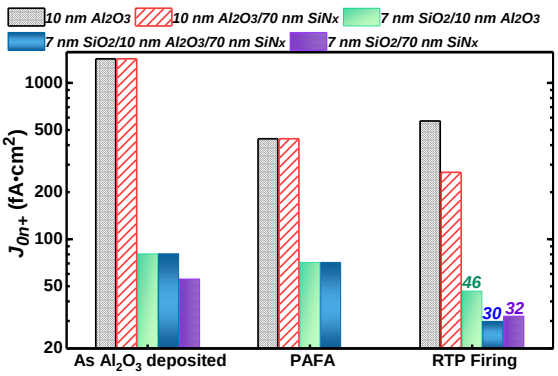

Fig. 4.

Fig. 3. Measured $J_{0,p+}$ (average) with different stacks as a function of the thermal processes. B-emitter parameters: N_{surf}≈1.2·10^{19} cm^{-3}, X_j≈2.82 µm, $R_{□}$=69 Ω/□.

Fig. 4. Measured $J_{0,n+}$ (average) with different stacks as a function of the thermal processes. P-emitter parameters: N_{surf}≈8.8·10^{19} cm^{-3}, X_j≈0.30 µm, $R_{□}$=100 Ω/□. The samples with the SiO_2/SiN_x stacks did not undergo the PAFA.

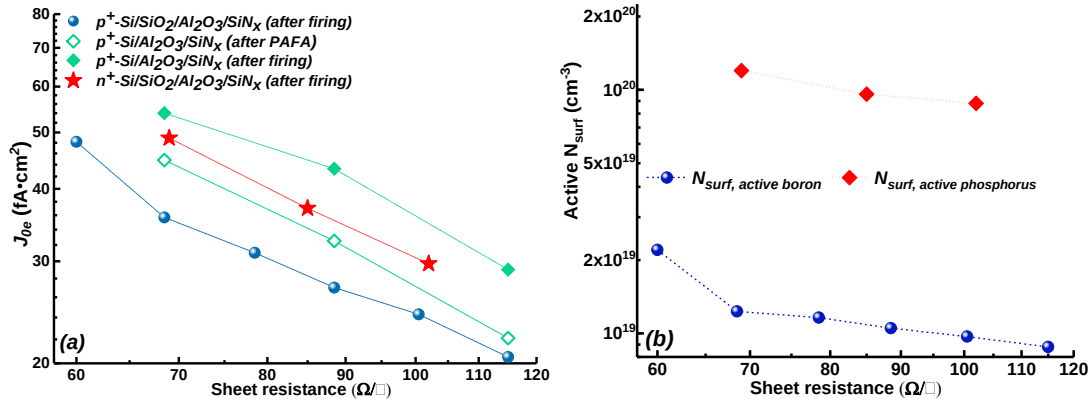

Fig. 5. Measured J_{0e} (a) and active N_{surf} (b) as a function of the $R_{□}$ and different stacks. The samples underwent the processes in Fig. 1. d_{film} of each layer is shown in Fig.s 3-4. The lines serve as a guide to the eye.

3.2 p^+ and n^+ emitter passivation mechanisms of $SiO_2/Al_2O_3/SiN_x$stacks

The effective passivation of p^+ and n^+ emitters using $SiO_2/Al_2O_3/SiN_x$ stacks should be linked to a good chemical passivation, a good field-effect passivation, or both. In this section, in order to further explain the lifetime results, we investigated the emitter passivation mechanisms of different dielectric stacks by combining experimental and simulation results.

3.2.1 Changes in field-effect and chemical passivation during the thermal processes

First we studied the changes in field-effect passivation of each stacks during the thermal processes by measuring Q_{eff} as shown in Fig. 6. It is seen that the Q_{eff} of Al_2O_3/(SiN_x) on both p^+ and n^+ emitter was -2.5·10^{12} cm^{-2} after PAFA; while a 7 nm SiO_2 interlayer decreased the negative Q_{eff} by a factor of 3.5 and 11.4 on p^+ and n^+ emitter, respectively. Further, after a full activation of the negative Q_f of Al_2O_3 by PAFA, the subsequent PECVD SiN_x and firing hardly affected Q_{eff}. A SiN_x capping layer on top of Al_2O_3 also did not affect Q_{eff}. The charge levels are similar between p^+ and n^+ emitters despite a slight difference. The results are consistent with Ref.s [27–31]. The tuning of Q_{eff} by the SiO_2 interlayer follows a model with two regimes as a function of d_{SiO2}, i.e. 1) dominated by the tunneling of electrons from Si through SiO_2 into Al_2O_3 defects states near SiO_2/Al_2O_3 interface for $d_{SiO2}<d_0$ (where d_0 is the threshold thickness

for zero-Q_{eff} of the $SiO_2/Al_2O_3/(SiN_x)$ stacks) and 2) dominated by charges intrinsic to the SiO_2 film for $d_{SiO2}>d_0$. Due to different positive Q_f in the SiO_2, different SiO_2 synthesis methods result in different d_0. In this study, 7 nm is lower than d_0 of thermally grown SiO_2, and thus the stacks show a negative Q_{eff}. The difference in Q_{eff} between p-Si and n-Si in case of $SiO_2/Al_2O_3/(SiN_x)$ is due to the different effective tunneling barrier thickness, which is caused by the different band structure formed at the Si/SiO_2 interface when band bending occurs due to the presence of built-in charges [28]. Additionally, as found in our unpublished study and consistent with Ref. [49], an excessive thermal budget could also reduce to some extent the already fully activated negative Q_f of Al_2O_3. In this study, the thermal budget of the subsequent remote PECVD SiN_x (400ºC, ~10 min process time) and RTP firing is acceptable and only very slightly reduced the negative Q_f of Al_2O_3 (from $-2.5\cdot10^{12}$ to $-2.4\cdot10^{12}$ cm^{-2}). Therefore, the Q_{eff} of the $(SiO_2)/Al_2O_3/(SiN_x)$ stacks was nearly unchanged in these thermal treatments.

In summary, for all stacks, the nearly unchanged Q_{eff} after the PAFA indicated a nearly unchanged field-effect passivation in the subsequent thermal processes, for both B and P emitter. Hence, the changes in emitter passivation quality (J_{0e}) are attributed mainly to the changes in chemical passivation. In order to gain further insights, calculations and simulations are reported in the following. Then, we discuss the parameters combining experimental results with simulations.

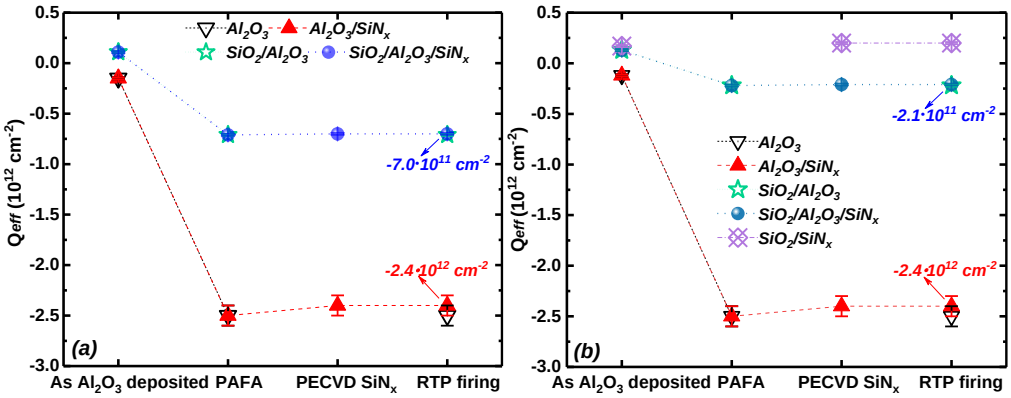

Fig. 6. The measured Q_{eff} of all stacks as a function of the thermal processes: Q_{eff} measured on (a) p-type and (b) n type Si substrate. Q_{eff} error is ~$1\cdot10^{10}$ ($1\cdot10^{11}$) cm^{-2} with the Q_{eff} in the order of 10^{11} (10^{12}) cm^{-2}. d_{film} of each layer as in Fig.s 3-4.

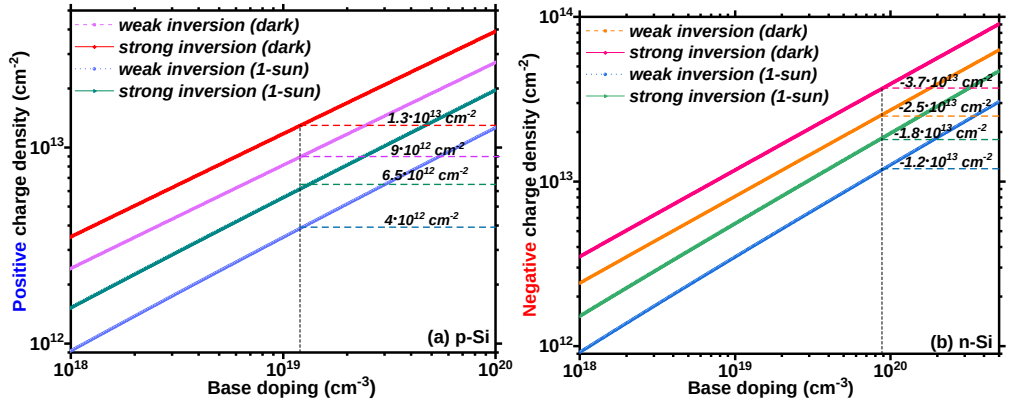

Fig. 7. Calculated threshold charge density (under dark and 1-sun illumination) for weak and strong inversion in p-Si (a) and n-Si (b) as a function of base doping density. The corresponding threshold charge density for inversion of the p^+ and n^+ emitter in this study (see the emitter parameters in Fig.s 3-4) have been marked.

Different Q_{eff} at Si/dielectrics interface can form an accumulation, depletion or inversion layer on Si surface, which induces different mechanisms of field-effect passivation [20]. An inversion induced field-effect passivation is undesirable in solar cells due to association with a lifetime reduction at low injection levels ($<10^{15}$ cm^3, within the operating regime of solar cells) as well as potential parasitic shunting [1,29,50]. Thus, we do not discuss this case here. In order to provide a necessary support for this study, a threshold charge density for weak and strong inversion in p- and n-Si as a function of base doping density was calculated (Fig. 7) by solving Poisson's equation in one dimension [20,51]. Considering the importance of both dark characteristics and practical operating conditions of solar cells, the calculation was performed at two typical conditions, i.e. under dark and under 1-sun illumination. According to Fig.s 6-7, the Q_{eff} in any of the stacks is not enough to invert the emitters in this study.

PC1D simulations were performed to investigate the changes in chemical passivation of each stack in the thermal processes. The updated PC1Dmod V6.2 software developed by Haug *et al.* [52] was used, which implements the most recent models mentioned in Ref.s [52–55]. After inputting substrate and emitter parameters, one of the following three parameters, S_n (or S_p), Q_{eff} and J_{0e}, was extracted by fixing the other two. The input Q_{eff} and J_{0e} were the measured results when they were used to extract the others. The surface recombination velocity for electrons (holes), S_n (S_p) is proportional to surface state density [1], and thus is determined by both N_{surf} and chemical passivation. Field-effect passivation is controlled by Q_{eff}. Using the above method, the S_n (S_p) as a function of the thermal processes and different stacks are shown in Fig.s 8-a and 9-a (corresponding to Fig.s 3 and 4, respectively). Here, the PC1D simulation error of S_n and S_p resulting from the error of the input Q_{eff} measured by COCOS is within 0.7% (4.8%) with Q_{eff} in the order of 10^{11} (10^{12}) cm^{-2}. The simulation error is small and thus not shown in the figures. To further understand the passivation mechanisms of different stacks, the simulated J_{0p+} (J_{0n+}) contour plot as a function of Q_{eff} and S_n (S_p) is shown in Fig. 8-b (9-b), which reveals the basic rules of the comprehensive effect of field-effect and chemical passivation on the overall emitter passivation (J_{0e}). In Fig. 8-b, typical combinations (a, b, c, d, e) of parameters of field-effect and chemical passivation to reach a J_{0p+} = 36 $fA \cdot cm^{-2}$ (the best J_{0p+} in Fig. 3) are marked, which will be discussed in Sec. 3.2.2.

Firstly, a further explanation on Fig. 3 (B emitter) is presented by combining with the analysis of Fig. 8. As discussed above, the changes in J_{0p+} with thermal processes are attributed mainly to the changes in chemical passivation (S_n). For the Al_2O_3/SiN_x stacks, the increased J_{0p+} from PAFA to post-firing is due to a decreased chemical passivation level with S_n increasing by a factor of 1.2. For the $SiO_2/Al_2O_3/SiN_x$ stacks, the decreased J_{0p+} from PAFA to post-firing is due to an improved chemical passivation with S_n decreasing by a factor of 3.75. Further, for the Al_2O_3/SiN_x stacks, the strong negative-charge field-effect passivation ($Q_{eff}\approx-2.4\cdot10^{12}$ cm^{-2}) dominates the surface passivation mechanism and also relaxes the requirements on chemical passivation (Fig. 8-b). However, J_{0p+} is not yet good enough due to a relatively poor chemical passivation after PAFA, which further worsens after firing. By comparison, for the $SiO_2/Al_2O_3/SiN_x$ stacks, the excellent post-fired J_{0p+} is due to an excellent chemical passivation ($S_n\approx3650$ $cm \cdot s^{-1}$) combined with a relatively weak negative-charge field-effect passivation ($Q_{eff}\approx-7.0\cdot10^{11}$ cm^{-2}). Thus, an important conclusion in Fig. 8-b is that, although a good level of field-effect (Q_{eff}) or chemical passivation (S_n) can strongly relax the requirements on the other one, a good emitter passivation still depends on their good combination.

It is also worth stressing that, a SiN_x capping layer can only suppress the deterioration degree in chemical passivation of Al_2O_3/p^+-Si interface, but it cannot prevent its deterioration. As shown in Fig. 8-a, the post-fired S_n decreases by a factor of 1.46 (from Al_2O_3 to Al_2O_3/SiN_x); while S_n still increases by a factor of 1.2 from after-PAFA Al_2O_3 to post-fired Al_2O_3/SiN_x. Hence, a SiN_x capping layer still cannot

effectively improve chemical passivation on its own, but it maintains the passivation mechanism of Al_2O_3. By comparison, the SiO_2 interlayer significantly improves chemical passivation, as well as changing the passivation mechanism. Overall, the $SiO_2/Al_2O_3/SiN_x$ stacks obtained the best post-fired J_{0p+} due to an excellent combination of chemical and field-effect passivation.

Likewise, a further explanation on Fig. 4 (P emitter) is given by combining with the analysis of Fig. 9. For the $SiO_2/Al_2O_3/SiN_x$ stacks (after firing), due to a weak field-effect passivation (Q_{eff}≈-2.1·10^{11} cm^{-2}), the excellent chemical passivation (S_p≈1000 cm·s^{-1}) plays a much more important role on the low J_{0n+}. The emitter passivation mechanism of SiO_2/SiN_x (Q_{eff}≈2·10^{11} cm^{-2}, S_p≈2220 cm·s^{-1}) is similar to $SiO_2/Al_2O_3/SiN_x$. The Al_2O_3 interlayer between SiO_2 and SiN_x can improve the chemical passivation. On the other hand, for the $Al_2O_3/(SiN_x)$ stacks, the negative Q_{eff} = -2.4·10^{12} cm^{-2} still cannot invert the n$^+$-Si surface (Fig. 7-b) and seriously depletes the n$^+$-Si surface, thus resulting in a poor J_{0n+}. Regarding the improvement in chemical passivation from PAFA to post-firing, the Al_2O_3/SiN_x, SiO_2/Al_2O_3, SiO_2/SiN_x and $SiO_2/Al_2O_3/SiN_x$ stacks decrease S_p by a factor of 2.3, 2.5, 7.8, 23.4, respectively. Here, a difference from the B emitter is that a SiN_x capping layer can effectively improve chemical passivation of Al_2O_3/n$^+$-Si interface. Furthermore, the post-fired S_p decreases by a factor of 4.2 (from Al_2O_3 to Al_2O_3/SiN_x) and 9.4 (from SiO_2/Al_2O_3 to $SiO_2/Al_2O_3/SiN_x$). Overall, the $SiO_2/Al_2O_3/SiN_x$ stacks obtained the best post-fired J_{0n+}.

As mentioned in the introduction, the improved firing stability of Al_2O_3 (i.e. the improved chemical passivation of Si interface by a thin SiO_2 interlayer, or the suppression of deterioration degree in chemical passivation of Al_2O_3/p$^+$-Si interface and the improved chemical passivation of Al_2O_3/n$^+$-Si interface by a SiN_x capping layer) is linked to H passivation provided by $(SiO_2)/Al_2O_3/(SiN_x)$ stacks [7,16,17,32–36]. This advantage can be further exploited by utilizing the back-end thermal processes (PECVD SiN_x, firing) of screen-printed Si solar cells. Considering the Q_{eff} tuning effect by the SiO_2 interlayer, $SiO_2/Al_2O_3/SiN_x$ has an excellent chemical passivation combined with a weak field-effect passivation, thus an excellent emitter (p$^+$ and n$^+$) passivation with an outstanding firing stability.

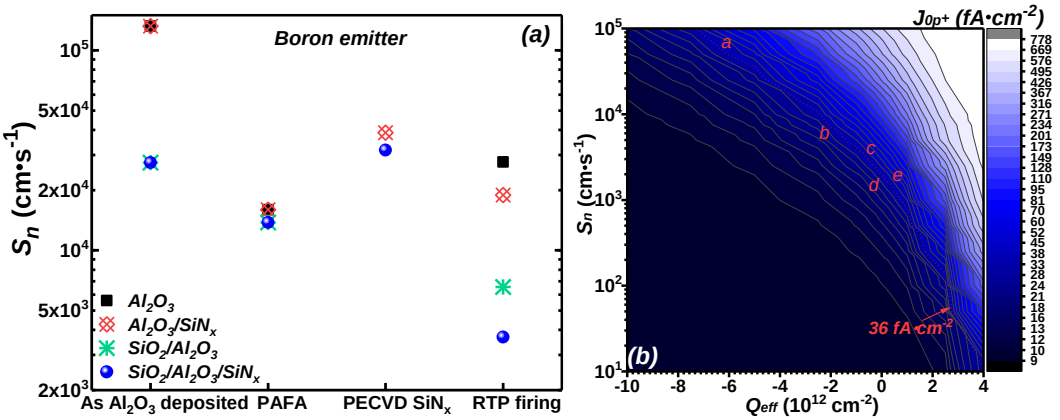

Fig. 8. The PC1D-extracted S_n as a function of the thermal processes and passivation stacks (a) and PC1D simulated J_{0p+} contour plot as a function of Q_{eff} and S_n (b). 1) B-emitter parameters and d_{film} of each layer are shown in Fig. 3; 2) The Q_{eff} range of -1.0·10^{13} to 4.0·10^{12} cm^{-2} cannot invert the p$^+$-Si surface in this study (both under dark and 1-sun illumination, see Fig. 7-a); 3) Typical combinations (a, b, c, d, e) of parameters of field-effect and chemical passivation to reach a J_{0p+} = 36 fA·cm^{-2} are marked (see Sec. 3.2.2).

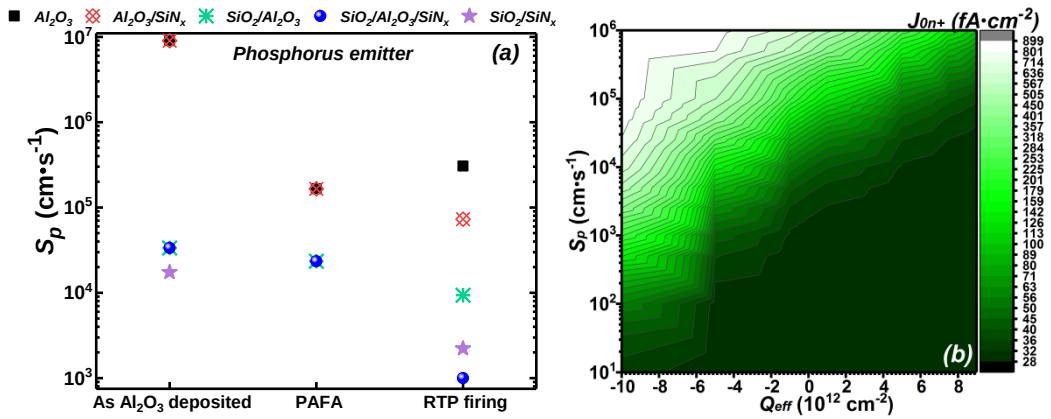

Fig. 9. The PC1D-extracted S_p as a function of the thermal processes and passivation stacks (a) and PC1D simulated J_{0n+} contour plot as a function of Q_{eff} and S_p (b). 1) P-emitter parameters and d_{film} of each layer are shown in Fig. 4; 2) The Q_{eff} range of $-1.0\cdot10^{13}$ to $9.0\cdot10^{12}$ cm^{-2} cannot invert the n$^+$-Si surface in this study (both under dark and 1-sun illumination, see Fig. 7-b).

3.2.2 Extended discussion on industrial emitter passivation

The same J_{0e} can be obtained from combinations of different levels of field-effect and chemical passivation, which is linked to different surface passivation mechanisms. J_{0p+} = 36 fA·cm^{-2} (the best J_{0p+} in Fig. 3) can be achieved with different dielectrics, as shown in Fig. 8-b. For example, with a) plasma ALD Al_2O_3 (Q_{eff}≈-6·10^{12} cm^{-2} [7], S_n≈6.3·10^4 cm·s^{-1}), b) thermal ALD Al_2O_3 in this study (Q_{eff}≈-2.4·10^{12} cm^{-2}, S_n≈1.1·10^4 cm·s^{-1}), c) $SiO_2/Al_2O_3/SiN_x$ in this study (Q_{eff}≈-7.0·10^{11} cm^{-2}, S_n≈3650 cm·s^{-1}), d) $SiO_2/Al_2O_3/SiN_x$ with adequate d_{SiO2} (zero Q_{eff}, S_n≈2200 cm·s^{-1}), or e) PECVD SiN_x (Q_{eff}≈7.5·10^{11} cm^{-2} [1], S_n≈1150 cm·s^{-1}). While the above S_n values have been reached with implanted B-emitters, it is worth to stress that the result of b) is also consistent with diffused B-emitters, e.g. Ma et al [56] obtained S_n≈1·10^4 cm·s^{-1} in a similar B_{surf} range with PECVD Al_2O_3/SiN_x stacks (Q_{eff} ≈-2.5·10^{12} cm^{-2}) using SENTAURUS TCAD simulations.

For industrial surface passivation on only n$^+$ or p$^+$ emitter, the preferred choice is to adopt suitable material with an excellent field-effect passivation, e.g. Al_2O_3 for p$^+$ emitter. The PC1D-extracted S_n (S_p) as a function of the $R_{\square}$ and different stacks (corresponding to Fig. 5) is shown in Fig. 10. It is seen that, although $Al_2O_3/(SiN_x)$ could well passivate p$^+$ emitter after PAFA over a broad emitter doping range, its chemical passivation is not yet good and could further worsen after firing despite being partly improved by SiN_x capping. Hence, Al_2O_3 passivation on p$^+$-Si cannot exploit its best potential in screen-printed industrial Si solar cells (see Sec. 3.3) unless chemical passivation can be sufficiently improved. A potential solution is to implement H passivation treatment (hydrogenation) [57–60]. Hydrogenation can be realized by placing wafers into a tool which provides H source, while simultaneously heating and illuminating wafers to accumulate sufficient energy for hydrogenation from the incident photons. It can passivate Si interfaces (dangling bonds or other defects) and Si bulk (crystallographic defects, B-O defects or contamination) based on different mechanisms, and can be applied to both single and multi c-Si (n or p type) solar cells. Here, for its application to $Al_2O_3/(SiN_x)$ passivation on p$^+$-Si, the hydrogenation treatment can be implemented after completion of cell fabrication to improve chemical passivation of Si interface as well as maintaining the strong negative-charge field-effect passivation, thus best exploiting the potential of Al_2O_3 passivation. Moreover, the H presented in Al_2O_3/SiN_x can also be utilized as H source. It is feasible to develop cost-effective and commercial prototypes (tools) to realize such hydrogenation process.

On the other hand, for solar cells with the p^+ emitter and n^+ BSF both placed at the cell rear (e.g. IBC), dielectrics with an excellent chemical passivation and a weak field-effect passivation (Q_{eff}-range: $-1\cdot10^{11}$ to $1\cdot10^{11}$ cm^{-2}) are the preferred choice, e.g. $SiO_2/(Al_2O_3)/SiN_x$. Emitters with lower N_{surf} are more easily suffering from depleted and inverter layers (Fig. 7), and thus relatively more sensitive to field-effect passivation. Thereby, the excellent chemical passivation of $SiO_2/Al_2O_3/SiN_x$ can greatly decrease the dependence on field-effect passivation, and it can thus effectively passivate both p^+ and n^+ emitters over a broad emitter doping range (Fig. 5). With increasing $R_{\square}$ in the ranges in Fig. 10, the $SiO_2/Al_2O_3/SiN_x$ stacks (after firing) have S_n (B emitter) decreasing from $5.7\cdot10^3$ to $1.9\cdot10^3$ $cm\cdot s^{-1}$, and S_p (P emitter) decreasing from $5.5\cdot10^3$ to $1\cdot10^3$ $cm\cdot s^{-1}$.

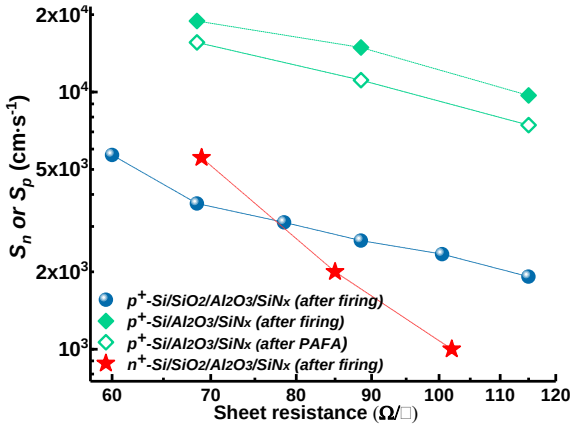

Fig. 10. The PC1D-extracted S_n (S_p) as a function of the $R_{\square}$ in different stacks. The active N_{surf} as a function of $R_{\square}$ is given in Fig. 5-b. d_{film} of each layer is shown in Fig.s 3-4.

3.3 Cell performance of p-PERT bifacial cells using $SiO_2/Al_2O_3/SiN_x$ emitter passivation

Based on the results of $SiO_2/Al_2O_3/SiN_x$ passivation of B and P emitters, we developed an industrial process (flow in Fig. 2-b) for p-PERT bifacial cells. Fig. 11 shows the front or rear side performance (under front or rear illumination only) of the cells fabricated in the industrial pilot line, which are well consistent with the J_{0e} results. The details on the groups in Fig. 11 are reported in Table 1. The better cell performance of group C_2 compared to group C_1 (for rear planar cells, $\Delta V_{oc}\approx$3-4 mV - V_{oc}, open circuit voltage, $\Delta\eta\approx$0.25%-0.3% - η, cell efficiency) confirmed the better final passivation on p^+ emitter with $SiO_2/Al_2O_3/SiN_x$ than with Al_2O_3/SiN_x. Similarly, the slightly better cell performance of group C_3 compared to group C_2 confirmed the slightly better final passivation on n^+ emitter with $SiO_2/Al_2O_3/SiN_x$ than with SiO_2/SiN_x.

In bifacial cells, it is necessary to evaluate both front and rear side performance, which can be quantified via the bifaciality factor *BF* ($BF=\eta_{rear}/\eta_{front}$), measured under standard test conditions [44]. As shown in Fig. 11, the front side performance of rear planar cells has a clear gain over rear textured cells ($\Delta V_{oc}\approx$3-4 mV, $\Delta\eta\approx$0.3-0.4%). This is due to better p^+-BSF and rear dielectric passivation, as well as better light trapping effect provided by the planar Si (100) surface [61]. On the other hand, the rear side performance of rear textured cells has significant advantage over rear planar cells (especially short circuit current J_{sc}) due to receiving more sunlight from the rear with lower reflectance. Overall, the cells demonstrated $\eta_{front}\approx$20.0-20.5% and $\eta_{rear}\approx$16.9-17.5% for rear planar cells and $\eta_{rear}\approx$19.0-19.8% for rear textured cells. Thus, the *BF* of the rear planar and rear textured cells are ~0.85 and ~0.98, respectively, with rear textured bifacial cells being more cost-efficient in actual environments.

The cell results also confirmed the effective emitter (p^+ and n^+) passivation using $SiO_2/Al_2O_3/SiN_x$ stacks. Based on our study, the substrate conductivity type is not critical for PERT bifacial cells since good cell performance can be achieved on both p and n substrates with a long enough bulk minority carrier diffusion length. It is worth stressing that, the cells with bifacial $SiO_2/Al_2O_3/SiN_x$ passivation on both p^+ and n^+ emitter (group C_3) achieved the best performance (V_{oc}=657 mV, η_{front}=20.5%, η_{rear}=19.8%, *BF*≈0.98). Due to the unique feature of bifacial Al_2O_3 deposition on Si substrates using ALD process and the combination with fully ion-implanted doping process, the cell process is clearly simplified. Better cell performance can be expected with further optimization of the front $SiO_2/Al_2O_3/SiN_x$ ARC layer and the specific Ag and Ag/Al pastes. In summary, the cell results demonstrate that $SiO_2/Al_2O_3/SiN_x$ is a promising candidate for industrial emitter passivation.

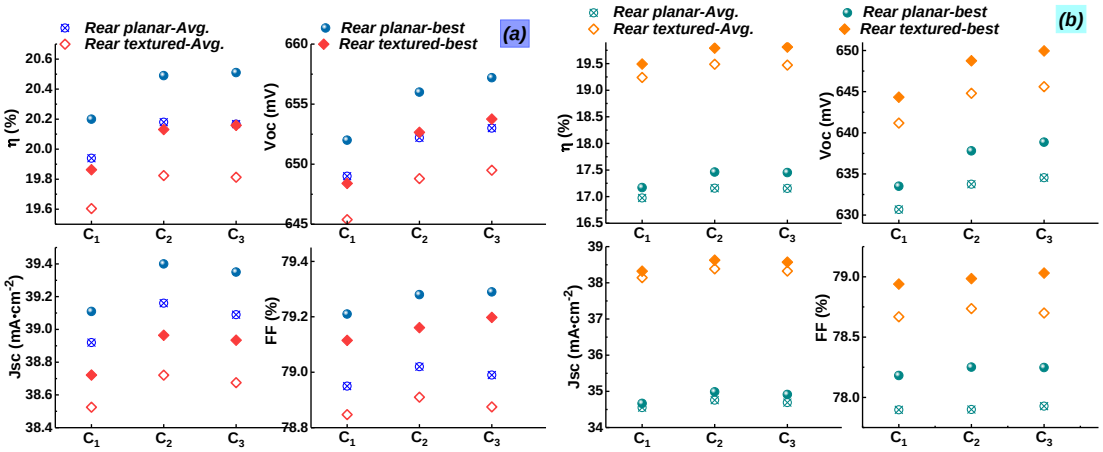

Fig. 11. Front (a) and rear (b) side performance of the industrial p-PERT bifacial cells (rear planar or textured surface) with different passivation stacks using the cell process in Fig. 2-b. Group information is given in Table 1.

Table 1. The group information in Fig. 11. The thicker d_{SiO2} of the front textured (111) Si surface compared to the rear planar (100) Si surface is due to a faster oxidation rate on the (111) Si compared to (100) Si.

Group	Front dielectrics	Rear dielectrics	Rear surface
C_1	10 nm SiO_2/67 nm SiN_x	10 nm Al_2O_3/70 nm SiN_x	planar or textured
C_2	10 nm SiO_2/67 nm SiN_x	7 nm SiO_2/10 nm Al_2O_3/70 nm SiN_x	
C_3	7 nm SiO_2/5 nm Al_2O_3/60 nm SiN_x	5 nm SiO_2/5 nm Al_2O_3/70 nm SiN_x	

4. Conclusion

In this paper, we have presented an emitter passivation scheme using $SiO_2/Al_2O_3/SiN_x$ stacks which can effectively passivate both p^+ and n^+ emitters. We systematically study the emitter passivation mechanisms of $SiO_2/Al_2O_3/(SiN_x)$ and $Al_2O_3/(SiN_x)$ stacks by characterizing the changes in both field-effect and chemical passivation due to different thermal processes, as well as the comprehensive effect of field-effect and chemical passivation on the overall emitter passivation (J_{0e}). We have shown that, after a full negative-charge activation by post-Al_2O_3 furnace anneal, the field-effect passivation of $(SiO_2)/Al_2O_3/(SiN_x)$ is nearly unchanged in the subsequent PECVD SiN_x and firing processes. The changes in J_{0e} are mainly due to the changes in chemical passivation. After firing, $SiO_2/Al_2O_3/SiN_x$ stacks had an excellent chemical passivation combined with a weak negative-charge field-effect passivation (Q_{eff}=-7.0·10^{11} cm^{-2} for p^+-Si, Q_{eff}=-2.1·10^{11} cm^{-2} for n^+-Si); while Al_2O_3/SiN_x stacks had a strong negative-charge field-effect passivation (Q_{eff}=-2.4·10^{12} cm^{-2}) combined with a poor chemical passivation. Furthermore, for $(SiO_2)/Al_2O_3/(SiN_x)$ passivation on p^+ and n^+ emitter, the SiO_2 interlayer can effectively improve chemical passivation of Si interface. By comparison, the SiN_x capping layer cannot prevent the

deterioration in chemical passivation of Al_2O_3/p^+-Si interface, but only suppressing its deterioration degree; while the SiN_x capping layer improves chemical passivation of Al_2O_3/n^+-Si interface. In addition, the excellent post-fired chemical passivation of $SiO_2/Al_2O_3/SiN_x$ due to hydrogen passivation can be further exploited by utilizing the back-end thermal processes of industrial screen-printed Si solar cells. Overall, $SiO_2/Al_2O_3/SiN_x$ can well passivate both p^+ and n^+ emitter over a broad emitter-doping range, as demonstrated by post-fired J_{0p+} = 20-50 fA·cm^{-2} and S_n = 1.9-5.7·10^3 cm·s^{-1} with $R_{\square B}$ (N_{surf})-range of 115-60 Ω/□ (8.8·10^{18}-2.2·10^{19} cm^{-3}), and post-fired J_{0n+} = 30-50 fA·cm^{-2} and S_p = 1·10^3-5.5·10^3 cm·s^{-1} with $R_{\square P}$ (N_{surf})-range of 100-70 Ω/□ (8.8·10^{19}-1.2·10^{20} cm^{-3}), respectively. We also propose that, to best exploit the advantage of Al_2O_3 passivation on p^+-Si, a hydrogenation treatment after completion of cell fabrication is a potential solution to improve chemical passivation of Si interface as well as maintaining the strong negative-charge field-effect passivation.

We also apply the above results to the industrial p-PERT bifacial cells and present an industrial roadmap based on $SiO_2/Al_2O_3/SiN_x$ emitter passivation combined with fully ion-implanted technology. Using this roadmap, industrial p-PERT bifacial cells have demonstrated good bifacial performance with η_{front} = 20.0-20.5%, η_{rear} = 19.0-19.8% (BF≈0.98) for rear textured cells and η_{rear} = 16.9-17.5% (BF≈0.85) for rear planar cells. The cells with bifacial $SiO_2/Al_2O_3/SiN_x$ passivation on both p^+ and n^+ emitters have also demonstrated promising cell performance and a simplified cell process.

Acknowledgment

The research work is based on the China-Finland International R&D Cooperation project "Improved cost-efficiency in crystalline silicon solar cells through Atomic Layer Deposited Al_2O_3", funded by MOST and TEKES (Finish Project No. 40843, Chinese Project No. S2013GR0622, 2013.05-2016.05). H Huang wishes to thank Intevac ltd. (especially Weicheng Zhu, Xiaochun Lu and Chunfeng Lu) for their help on using the ENERGi implanters and the optimization of the ion implantation processes in this study. T. P. Pasanen acknowledges the Aalto ELEC Doctoral School and Jenny and Antti Wihuri Foundation for the financial support.

Reference

[1] A.G. Aberle, Crystalline silicon solar cell-Advanced surface passivation and analysis, Centre for Photovoltaic Engineering, Univ. of New South Wales, Sydney NSWS2052, Australia, Sydney, 1999.

[2] M.J. Kerr, Surface, Emitter and Bulk Recombination in Silicon and Development of Silicon Nitride Passivated Solar Cells, Australian National University, 2002.

[3] F. Chen, T. Li, J. Cotter, PECVD Silicon Nitride Surface Passivation for High-Efficiency N-Type Silicon Solar Cells, in: 2006 IEEE 4th World Conf. Photovolt. Energy Conf., IEEE, Hawaii, 2006: pp. 1020–1023.

[4] B. Hoex, J.J.H. Gielis, M.C.M. van de Sanden, W.M.M. Kessels, On the c-Si surface passivation mechanism by the negative-charge-dielectric Al2O3, J. Appl. Phys. 104 (2008) 113703.

[5] B. Hoex, J. Schmidt, P. Pohl, M.C.M. van de Sanden, W.M.M. Kessels, Silicon surface passivation by atomic layer deposited Al2O3, J. Appl. Phys. 104 (2008) 044903.

[6] J. Benick, B. Hoex, M.C.M. van de Sanden, W.M.M. Kessels, O. Schultz, S.W. Glunz, High efficiency n-type Si solar cells on Al2O3-passivated boron emitters, Appl. Phys. Lett. 92 (2008) 253504.

[7] G. Dingemans, E. Kessels, Status and prospects of Al2O3-based surface passivation schemes for silicon solar cells, J. Vac. Sci. Technol. A Vacuum, Surfaces Film. 30 (2012) 1–27.

[8] J. Schmidt, A. Merkle, R. Bock, P.P. Altermatt, A. Cuevas, N.-P. Harder, B. Hoex, R. van de Sanden, E. Kessels, R. Brendel, Progress in the surface passivation of silicon solar cells, in: 23rd Eur. Photovolt. Sol. Energy Conf., Valencia, 2008: pp. 974–981.

[9] Richard Roland. King, Studies of oxide-passivated emitters in silicon and applications to solar cells, Stanford university, 1990.

[10] A. Wang, High efficiency PERC and PERL Silicon solar cells, Univ. of New South Wales, Sydney, 1992.

[11] J. Zhao, A. Wang, M.A. Green, 24·5% Efficiency silicon PERT cells on MCZ substrates and 24·7% efficiency PERL cells on FZ substrates, Prog. Photovoltaics Res. Appl. 7 (1999) 471–474.

[12] J. Zhao, A. Wang, Rear emitter n-type passivated emitter, rear totally diffused silicon solar cell structure,

Appl. Phys. Lett. 88 (2006) 2006–2008.
[13] A.W. Blakers, A. Wang, A.M. Milne, J. Zhao, M.A. Green, 22.8% Efficient Silicon Solar Cell, Appl. Phys. Lett. 55 (1989) 1363–1365.
[14] D.D. Smith, P.J. Cousins, A. Masad, S. Westerberg, M. Defensor, T. Dennis, R. Daquin, N. Bergstrom, A. Leygo, X. Zhu, B. Meyers, M. Shields, D. Rose, SunPower's Maxeon Gen III solar cell:High Efficiency and Energy Yield, in: IEEE 39th Photovolt. Spec. Conf., Tampa, 2013: pp. 0908–0913.
[15] S. Duttagupta, F.J. Ma, B. Hoex, A.G. Aberle, Excellent surface passivation of heavily doped p+ silicon by low-temperature plasma-deposited SiOx/SiNy dielectric stacks with optimised antireflective performance for solar cell application, Sol. Energy Mater. Sol. Cells. 120 (2014) 204–208.
[16] A. Richter, J. Benick, M. Hermle, S.W. Glunz, Excellent silicon surface passivation with 5 Å thin ALD Al2O3 layers: Influence of different thermal post-deposition treatments, Phys. Status Solidi - Rapid Res. Lett. 5 (2011) 202–204.
[17] J. Schmidt, B. Veith, R. Brendel, Effective surface passivation of crystalline silicon using ultrathin Al2O3 films and Al2O3/SiNx stacks, Phys. Status Solidi - Rapid Res. Lett. 289 (2009) 287–289.
[18] T.C. Kho, L.E. Black, K.R. McIntosh, Degradation of Si-SiO2 interfaces during rapid thermal annealing, in: 24th Eur. Photovolt. Sol. Energy Conf. Exhib., Hamburg, 2009: pp. 21–25.
[19] M.C. Talló, K.R. Mcintosh, Permeability of TiO2 antireflection coatings to damp heat, in: 24th Eur. Photovolt. Sol. Energy Conf., Hamburg, 2009: pp. 2037–2040.
[20] S.M. Sze, K.K. Ng, Physics of semiconductor devices, 3rd Editio, Wiley-Interscience, 2007.
[21] G. Dingemans, P. Engelhart, R. Seguin, F. Einsele, B. Hoex, M.C.M. van de Sanden, W.M.M. Kessels, Stability of Al2O3 and Al2O3/a-SiNx:H stacks for surface passivation of crystalline silicon, J. Appl. Phys. 106 (2009) 114907.
[22] B. Vermang, H. Goverde, A. Lorenz, A. Uruena, G. Vereecke, J. Meersschaut, E. Cornagliotti, A. Rothschild, J. John, J. Poortmans, others, On the blistering of atomic layer deposited Al2O3 as Si surface passivation, in: Proc. 37th IEEE Photovolt. Spec. Conf., 2011: pp. 3562–3567.
[23] S. Li, P. Repo, G. Von Gastrow, Y. Bao, H. Savin, Effect of ALD reactants on blistering of aluminum oxide films on crystalline silicon, in: Conf. Rec. IEEE Photovolt. Spec. Conf., 2013: pp. 1265–1267.
[24] J. Chen, E. Cornagliotti, X. Loozen, E. Simoen, J. Vanhellemont, J. Lauwaert, H. Vrielinck, J. Poortmans, Impact of firing on surface passivation of p-Si by SiO2/Al and SiO2/SiNx/Al stacks, J. Appl. Phys. 110 (2011) 126101.
[25] M. Hofmann, S. Kambor, C. Schmidt, D. Grambole, J. Rentsch, S.W. Glunz, R. Preu, PECVD-ONO: A new deposited firing stable rear surface passivation layer system for crystalline silicon solar cells, Adv. Optoelectron. 2008 (2008) 10.
[26] G. Dingemans, M.M. Mandoc, S. Bordihn, M.C.M. Van De Sanden, W.M.M. Kessels, Effective passivation of Si surfaces by plasma deposited SiO x/a-SiNx:H stacks, Appl. Phys. Lett. 98 (2011) 1–4.
[27] G. Dingemans, N.M. Terlinden, M.A. Verheijen, M.C.M. Van De Sanden, W.M.M. Kessels, Controlling the fixed charge and passivation properties of Si(100)/Al2O3 interfaces using ultrathin SiO2 interlayers synthesized by atomic layer deposition, J. Appl. Phys. 110 (2011).
[28] N.M. Terlinden, G. Dingemans, V. Vandalon, R.H.E.C. Bosch, W.M.M. Kessels, Influence of the SiO2 interlayer thickness on the density and polarity of charges in Si/SiO2/Al2O3 stacks as studied by optical second-harmonic generation, J. Appl. Phys. 115 (2014) 033708.
[29] B.W.H.W.H. van de Loo, H.C.M.C.M. Knoops, G. Dingemans, G.J.M.J.M. Janssen, M.W.P.E.W.P.E. Lamers, I.G.G. Romijn, A.W.W. Weeber, W.M.M.M.M. Kessels, "Zero-charge" SiO2/Al2O3 stacks for the simultaneous passivation of n+ and p+ doped silicon surfaces by atomic layer deposition, Sol. Energy Mater. Sol. Cells. 143 (2015) 450–456.
[30] S. Mack, A. Wolf, C. Brosinsky, S. Schmeisser, A. Kimmerle, P. Saint-cast, M. Hofmann, D. Biro, Silicon Surface Passivation by Thin Thermal Oxide/PECVD Layer Stack Systems, IEEE J. Photovoltaics. 1 (2011) 135–145.
[31] J. a. Aboaf, D.R. Kerr, E. Bassous, Charge in SiO2-Al2O3 Double Layers on Silicon, J. Electrochem. Soc. 120 (1973) 1103.
[32] G. Dingemans, M.C.M. van de Sanden, W.M.M. Kessels, Excellent Si surface passivation by low temperature SiO2 using an ultrathin Al2O3 capping film, Phys. Status Solidi - Rapid Res. Lett. 5 (2011) 22–24.
[33] G. Dingemans, M.C.M. van de Sanden, W.M.M. Kessels, Influence of the Deposition Temperature on the c-Si Surface Passivation by Al2O3 Films Synthesized by ALD and PECVD, Electrochem. Solid-State Lett. 13 (2010) H76.
[34] G. Dingemans, F. Einsele, W. Beyer, M.C.M. Van De Sanden, W.M.M. Kessels, Influence of annealing and Al_2O_3 properties on the hydrogen-induced passivation of the Si/SiO_2 interface, J. Appl. Phys. 111

(2012).
[35] G. Dingemans, W. Beyer, M.C.M. van de Sanden, W.M.M. Kessels, Hydrogen induced passivation of Si interfaces by Al2O3 films and SiO2/Al2O3 stacks, Appl. Phys. Lett. 97 (2010) 152106.
[36] V. Naumann, M. Otto, R.B. Wehrspohn, C. Hagendorf, Chemical and structural study of electrically passivating Al2O3/Si interfaces prepared by atomic layer deposition, J. Vac. Sci. Technol. A Vacuum, Surfaces, Film. 30 (2012) 04D106.
[37] E. Simoen, A. Rothschild, B. Vermang, J. Poortmans, R. Mertens, Impact of Forming Gas Annealing and Firing on the Al2O3/p-Si Interface State Spectrum, Electrochem. Solid-State Lett. 14 (2011) 2011–2013.
[38] S. Bordihn, P. Engelhart, V. Mertens, G. Kesser, High surface passivation quality and thermal stability of ALD Al2O3 on wet chemical grown ultra-thin SiO2 on silicon, Energy Procedia. 00 (2011) 17–20.
[39] S. Bordihn, G. Dingemans, V. Mertens, W.M.M. Kessels, Passivation of n+-Type Si Surfaces by Low Temperature Processed SiO2/Al2O3 Stacks, IEEE J. Photovoltaics. 3 (2013) 925–929.
[40] T. Pasanen, V. Vähänissi, N. Theut, H. Savin, Surface passivation of black silicon phosphorus emitters with atomic layer deposited SiO2/Al2O3 stacks, Energy Procedia. 124 (2017) 307–312.
[41] B.W.H. Van De Loo, A. Ingenito, M.A. Verheijen, O. Isabella, M. Zeman, W.M.M. Kessels, Surface passivation of n-type doped black silicon by atomic-layer-deposited SiO2/Al2O3 stacks, Appl. Phys. Lett. 110 (2017).
[42] F. Lin, S. Duttagupta, K.D. Shetty, M. Boreland, A.G. Aberle, B. Hoex, Excellent passivation of p+ silicon surfaces by inline plasma enhanced chemical vapor deposited SiOx/AlOx stacks, Jpn. J. Appl. Phys. 51 (2012).
[43] T. Dullweber, C. Kranz, R. Peibst, U. Baumann, H. Hannebauer, A. Fülle, S. Steckemetz, T. Weber, M. Kutzer, M. Müller, G. Fischer, P. Palinginis, and H Neuhaus, PERC^{+}: industrial PERC solar cells with rear Al grid enabling bifaciality and reduced Al paste consumption, Prog. Photovolt Res. Appl. 24 (2016) 1487–1498.
[44] P. Ooshaksaraei, K. Sopian, R. Zulkifli, M.A. Alghoul, S.H. Zaidi, Characterization of a bifacial photovoltaic panel integrated with external diffuse and semi mirror type reflectors, Int. J. Photoenergy. (2013) 465837.
[45] M.C.U. Stm, User Manual of "WCT-120 Photo-conductance Lifetime Tester and optional Suns-V_{oc}", 2007.
[46] D.E. KANE, R.M. SWANSON, Measurement of the emitter saturation current by a contactless photoconductivity decay method, in: IEEE Photovolt. Spec. Conf. 18, 1985: pp. 578–583.
[47] A.W. Stephens, M.A. Green, Effectiveness of 0.08 molar iodine in ethanol solution as a means of chemical surface passivation for photoconductance decay measurements, Sol. Energy Mater. Sol. Cells. 45 (1997) 255–265.
[48] https://www.semilab.hu/products/pvi/pv-2000, https://www.semilab.hu/products/si/faast-cocos-mc.
[49] J. Benick, A. Richter, T.T.A. Li, N.E. Grant, K.R. Mcintosh, Y. Ren, K.J. Weber, M. Hermle, S.W. Glunz, Effect of a post-deposition anneal on Al2O3/Si interface properties, in: Photovolt. Spec. Conf. (PVSC), 2010 35th IEEE, Honolulu, 2010: pp. 000891–000896.
[50] M.A. Green, Silicon Solar Cells: Advanced Principles and Practice, Univ. of New South Wales, Sydney, 1995.
[51] G. Von Gastrow, R. Alcubilla, P. Ortega, M. Yli-Koski, S. Conesa-Boj, A. Fontcuberta I Morral, H. Savin, Analysis of the Atomic Layer Deposited Al2O3 field-effect passivation in black silicon, Sol. Energy Mater. Sol. Cells. 142 (2015) 29–33.
[52] H. Haug, A. Kimmerle, J. Greulich, A. Wolf, E. Stensrud Marstein, Implementation of Fermi-Dirac statistics and advanced models in PC1D for precise simulations of silicon solar cells, Sol. Energy Mater. Sol. Cells. 131 (2014) 30–36.
[53] A. Schenk, Finite-temperature full random-phase approximation model of band gap narrowing for silicon device simulation, J. Appl. Phys. 84 (1998) 3684–3695.
[54] D. Yan, A. Cuevas, Empirical determination of the energy band gap narrowing in p+ silicon heavily doped with boron, J. Appl. Phys. 116 (2014).
[55] D. Yan, A. Cuevas, Empirical determination of the energy band gap narrowing in highly doped n+ silicon, J. Appl. Phys. 114 (2013).
[56] F.J. Ma, S. Duttagupta, M. Peters, G.S. Samudra, A.G. Aberle, B. Hoex, Numerical modelling of silicon p+ emitters passivated by a PECVD AlOx/SiNx stack, Energy Procedia. 33 (2013) 104–109.
[57] S.R. Wenham, P.G. Hamer, B.J. Hallam, A. Sugianto, C.E. Chan, L. Song, P.H. Lu, A.M. Wenham, L. Mai, C.M. Chong, G. Xu, M. Edwards, Advanced hydrogenation of silicon solar cells, 2013.
[58] B. Hallam, M. Abbott, N. Nampalli, P. Hamer, S. Wenham, Influence of the formation-And passivation rate of boron-oxygen defects for mitigating carrier-induced degradation in silicon within a hydrogen-based model, J. Appl. Phys. 119 (2016) 1–11.

[59] B. Hallam, C. Chan, M. Abbott, S. Wenham, Hydrogen passivation of defect-rich n-type Czochralski silicon and oxygen precipitates, Sol. Energy Mater. Sol. Cells. 141 (2015) 125–131.
[60] C.E. Chan, D.N.R. Payne, B.J. Hallam, M.D. Abbott, T.H. Fung, A.M. Wenham, B.S. Tjahjono, S.R. Wenham, Rapid Stabilization of High-Performance Multicrystalline P-type Silicon PERC Cells, IEEE J. Photovoltaics. 6 (2016) 1473–1479.
[61] S.W. Glunz, High-Efficiency Crystalline Silicon Solar Cells, Adv. Optoelectron. 2007 (2007) Article ID 97370.